The Astrophysical Journal, 816:83 (8pp), 2016 January 10 doi:10.3847/0004-637X/816/2/83


# A MATURE GALAXY CLUSTER AT $z = 1.58$ AROUND THE RADIO GALAXY 7C 1753+6311

E. A. Cooke[1], N. A. Hatch[1], D. Stern[2], A. Rettura[3], M. Brodwin[4], A. Galametz[5], D. Wylezalek[6], C. Bridge[2,7], C. J. Conselice[1], C. De Breuck[8], A. H. Gonzalez[9], and M. Jarvis[10,11]

[1] School of Physics and Astronomy, University of Nottingham, University Park, Nottingham NG7 2RD, UK; Elizabeth.Cooke@nottingham.ac.uk
[2] Jet Propulsion Laboratory, California Institute of Technology, Pasadena, CA 91109, USA
[3] Infrared Processing and Analysis Center, California Institute of Technology, Pasadena, CA 91125, USA
[4] Department of Physics and Astronomy, University of Missouri, Kansas City, MO 64110, USA
[5] Max-Planck-Institut fuer Extraterrestrische Physik, Giessenbachstrasse, D-85748 Garching, Germany
[6] Department of Physics and Astronomy, Johns Hopkins University, 3400N. Charles St, Baltimore, MD 21218, USA
[7] California Institute of Technology, 1200 E. California Blvd., Pasadena, CA 91125, USA
[8] European Southern Observatory, Karl Schwarzschild Strasse 2, D-85748 Garching bei Munchen, Germany
[9] Department of Astronomy, University of Florida, Gainesville, FL 32611, USA
[10] Astrophysics, University of Oxford, Denys Wilkinson Building, Keble Road, Oxford OX1 3RH, UK
[11] Physics Department, University Of The Western Cape, Bellville, South Africa

*Received 2015 September 21; accepted 2015 November 10; published 2016 January 14*

## ABSTRACT

We report on the discovery of a $z = 1.58$ mature cluster around the high-redshift radio galaxy 7C 1753+6311, first identified in the Clusters Around Radio-loud active galactic nuclei survey. Two-thirds of the excess galaxies within the central 1 Mpc lie on a red sequence with a color that is consistent with an average formation redshift of $z_f \sim 3$. We show that $80 \pm 6\%$ of the red sequence galaxies in the cluster core are quiescent, while the remaining 20% are red due to dusty star formation. We demonstrate that the cluster has an enhanced quiescent galaxy fraction that is three times that of the control field. We also show that this enhancement is mass dependent: $91 \pm 9\%$ of the $M_* > 10^{10.5} M_\odot$ cluster galaxies are quiescent, compared to only $36 \pm 2\%$ of field galaxies, whereas the fraction of quiescent galaxies with lower masses is the same in the cluster and field environments. The presence of a dense core and a well-formed, quiescent red sequence suggest that this is a mature cluster. This means that distant radio galaxies do not solely reside in young, uncollapsed protoclusters, rather they can be found in clusters in a wide range of evolutionary states.

*Key words:* galaxies: clusters: individual (CARLA J1753+6311) – galaxies: evolution – galaxies: formation – galaxies: high-redshift – galaxies: individual (7C 1753+6311)

## 1. INTRODUCTION

To understand the formation history of galaxies in the densest environments, clusters, it is important to study their progenitors: high-redshift protocluster galaxies. Several techniques are now employed to locate clusters and protoclusters at $z > 1$, such as large photometric surveys (e.g., Chiang et al. 2014; Stanford et al. 2014), surveys exploiting the Sunyaev–Zel'dovich (SZ) effect (e.g., Hasselfield et al. 2013; Bleem et al. 2015; Planck Collaboration et al. 2015), and X-ray detections of the intracluster medium (ICM; e.g., Willis et al. 2013). Unfortunately, many of these methods are expensive, requiring deep coverage of large fields-of-view in order to locate the rare overdensities. Massive clusters have been found with the SZ effect out to $z \sim 1.5$, with a few candidates at even higher redshifts (e.g., Tozzi et al. 2015, see also Brodwin et al. 2012). These, however, are rare systems; SZ and X-ray surveys struggle to find the more typical, lower mass clusters at $z > 1.5$ since the signal from these methods scales with cluster mass. The high-redshift progenitors of the majority of local $M \sim 10^{14} M_\odot$clusters will be missed since they lack sufficiently massive cluster cores at $z \gtrsim 1.5$ to be detectable with current instruments (Chiang et al. 2013; Muldrew et al. 2015). A targeted approach reduces the strain on telescope time and can pinpoint clusters even at the highest redshifts. However, the right beacon needs to be used.

Radio-loud active galactic nuclei (RLAGN) preferentially reside in dense environments at high redshift (e.g., Galametz et al. 2012; Wylezalek et al. 2013), which are significantly denser than the environments of radio-quiet galaxies of the same stellar mass (Hatch et al. 2014), which is also predicted from models (Orsi et al. 2015). These RLAGN provide one of the most efficient ways to find and study large-scale structure formation, particularly at the highest redshifts. However, if RLAGN preferentially reside in clusters of a certain age or stage of collapse, then our view of cluster formation will be biased. For example, Simpson & Rawlings (2002) and van Breukelen (2009) suggest distant radio galaxies pinpoint merging clusters.

Most confirmed cluster progenitors, known as protoclusters, have been identified with Ly$\alpha$ emitters, H$\alpha$ emitters, or Lyman-break galaxies, which are tracers of young systems (e.g., Overzier et al. 2005; Venemans et al. 2007; Cooke et al. 2014). So the methods by which protoclusters have been identified preferentially pinpoint young, forming galaxies, and clusters that contain mature, passively evolving galaxies may be missed.

By contrast, large cluster surveys using *Spitzer* data are not intrinsically biased to star-forming galaxies (Simpson & Eisenhardt 1999; Eisenhardt et al. 2008; Muzzin et al. 2009; Galametz et al. 2012; Wylezalek et al. 2013; Rettura et al. 2014). The criterion proposed by Papovich (2008) uses a 3.6–4.5 $\mu$m color selection to isolate all types of galaxies at $z > 1.3$, thanks to the peak of stellar emission near 1.6 $\mu$min galaxy spectral energy distributions (SEDs) moving into these bands at $z > 1$. This feature is present in galaxies of all types so selecting only on this criteria does not greatly bias the galaxy selection.

One very successful *Spitzer* survey is the Clusters Around Radio-loud AGN survey (CARLA; Wylezalek et al. 2013,

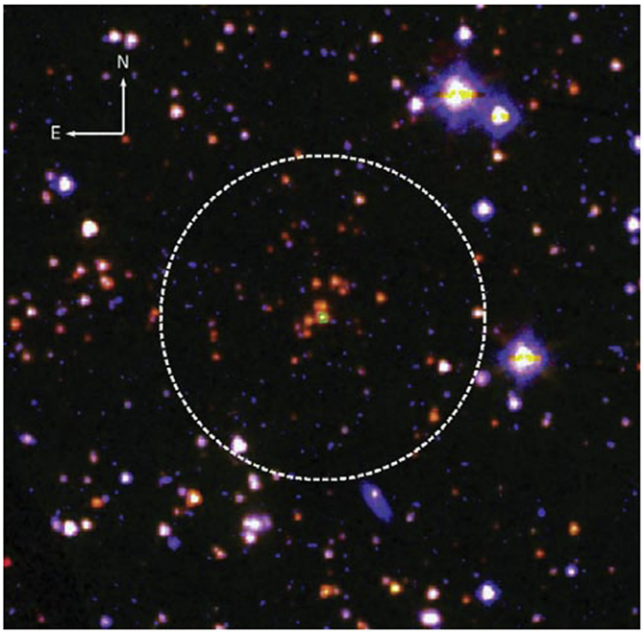


**Figure 1.** $i'$, [3.6], [4.5] three-color image of the field around 7C 1753+6311. The central RLAGN is marked with a green square. There are several red sources clustered around the RLAGN. The white dashed circle shows a 0.9 arcmin radius around the RLAGN. 0.9 arcmin at $z = 1.58$ corresponds to 0.46 Mpc in physical coordinates.

2014), which imaged over 400 fields surrounding RLAGN, and identified ∼200 cluster and protocluster candidates at $1.3 < z < 3.2$. Using the *Spitzer* wavebands to select both star-forming and passively evolving cluster members, these clusters can be used to investigate whether RLAGN are biased tracers of clusters that reside preferentially in younger structures, or whether the young structures discovered to date are due to the protocluster confirmation techniques used.

Based on deep optical imaging, Cooke et al. (2015) identified a subset of the densest CARLA fields that show signs of being mature clusters, exhibiting red sequences, and dense cores of red galaxies. Here we examine one of these fields, around the RLAGN 7C 1753+6311 (Figure 1). Lacy et al. (1999) tentatively assigned a redshift to this galaxy of $z = 1.95$ based on an uncertain emission line at 4854 Å assumed to be He II $\lambda$1640 and the possible detection of an associated Ly$\alpha$ break. This redshift was assigned a quality "$\gamma$," indicating an "uncertain" redshift. Here we report the first robust spectroscopic redshift for 7C 1753+6311, confirming it to instead be at $z = 1.58$, and examine the surrounding cluster environment. Section 2 outlines our data and methods used. In Section 3 we present a new, deep, optical spectrum of 7C 1753 +6311 which confirms its redshift as being $z = 1.58$. Section 4 then investigates the properties of the galaxies surrounding 7C 1753+6311, and Section 5 presents our conclusions.

In the following, all magnitudes and colors are in the AB photometric system and we assume a ΛCDM cosmology with $H_0 = 70\ \mathrm{km\ s^{-1}\ Mpc^{-1}}$, $\Omega_m = 0.3$, and $\Omega_\Lambda = 0.7$.

## 2. DATA AND METHOD

### 2.1. Imaging

The field surrounding 7C 1753+6311 was imaged with *Spitzer*'s Infrared Array Camera (IRAC; Fazio et al. 2004) at 3.6 and 4.5 $\mu$m by the CARLA survey (Wylezalek et al. 2013), reaching a $3\sigma$ depth of 23.8 mag and 24.4 mag at 3.6 $\mu$m and 4.5 $\mu$m, respectively. This field was identified as a protocluster candidate with a $4.5\sigma$ overdensity by Wylezalek et al. (2013) and was followed up in $i'$ and $J$ using the William Herschel Telescope in La Palma. The $i'$ band image was taken with the auxiliary-port camera (ACAM), with an exposure time of 6000 s. Full details of the $i'$ data are available in Cooke et al. (2015). The $J$ band image was obtained with the long-slit intermediate resolution infrared spectrograph (LIRIS), with an exposure time of 8160 s, and reduced in the standard way using the publicly available program THELI (Erben et al. 2005; Schirmer 2013). A $3\sigma$ depth is reached at $i' = 26.0$ mag and $J = 23.6$ mag, with seeing of ∼0.76 arcsec for both images.

The IRAC images have a much broader point-spread function (PSF) than the $i'$ and $J$ images, so selecting sources using the 4.5 $\mu$m image is prone to blending and some galaxies may be missed which are distinct in the $i'$ or $J$ bands. Using solely the $i'$ band to detect sources would result in biasing the selection toward intrinsically blue sources, whereas the $J$ image is relatively shallow, so we use a deep F140W image as a detection image. The field around 7C 1753+6311 was imaged with the F140W filter of the *Hubble Space Telescope* Wide-Field Camera 3 (*HST*/WFC3) in 2015 July as part of an on-going 40-orbit spectroscopic program (P.I. D. Stern). The *HST* spectra and photometry will be discussed in a future paper (G. Noirot et al. 2016, in preparation). We retrieved the calibrated, dither-combined (drizzled) image from MAST[12] to use as a detection image. This image has 0.5 ks exposure and is complete[13] to at least 24 mag.

Source extraction was done with SExtractor (Bertin & Arnouts 1996) in dual-image mode. The *HST* F140W detection image was used to detect sources, and photometry was obtained on the $i'$, $J$, 3.6, and 4.5 $\mu$m images in 2 arcsec diameter apertures. We are unable to use large apertures to measure the IRAC fluxes (e.g., 4 arcsec) due to the high spatial density of sources in the cluster core (galaxies are typically ∼2 arcsec apart). So we measure the fluxes in 2 arcsec diameter apertures and correct for the broader PSF of the IRAC data compared to the ground-based data using the ratio of the flux in the $J$ band image to the $J$ image convolved with a Gaussian kernel matching the IRAC PSF, following Hartley et al. (2013). Fluxes were corrected to total fluxes using the growth curves of bright, unsaturated stars in the field of view. This method assumes that the blended sources have the same $J$ − IRAC color, so may provide inaccurate colors for some sources.

### 2.2. High Redshift Galaxy Selection

To select sources likely to lie at high redshift, we employ two color cuts. The well-tested IRAC cut of $[3.6] - [4.5] > -0.1$ (Papovich 2008) selects sources at $z > 1.3$ due to the 1.6 $\mu$m peak of stellar emission moving into the IRAC bands at these redshifts. This cut was adjusted to $[3.6] - [4.5] > -0.2$ in order to be sure of selecting as complete a cluster sample as possible, although this also allows more lower-redshift sources to contaminate the sample. Most stars have $[3.6] - [4.5] \sim -0.5$ and so will be removed by this cut (Galametz et al. 2012). A second cut of $i' - [3.6] > -0.5 \times [3.6] + 11.4$ (Cooke et al. 2015) was

[12] Mikulski Archive for Space Telescopes: https://archive.stsci.edu.

[13] The histogram of number counts per magnitude bin starts to decrease after 25 mag in F140W.

applied to further remove bright low-redshift interlopers and contaminating AGN. To remove faint sources with potentially inaccurate flux measurements, only those with magnitudes brighter than 23.8 mag in 4.5 $\mu$m ($5\sigma$ image depth) and 23.6 mag in $J$ ($3\sigma$ image depth) were considered. Any sources referred to hereafter are those that match these criteria. To maximise the overdensity of (proto)cluster sources to field contaminants, we only consider sources within 0.9 arcmin of the central RLAGN.

The completeness of our catalog is a function of F140W magnitude. This image is deeper than the ground-based imaging and is 100% complete to the $J$ band limit of 23.6 mag.

### 2.3. Statistical Subtraction

#### 2.3.1. Control Field

Throughout this study, we use the eighth data release (DR8) of the UKIDSS Ultra Deep Survey (UDS; Hartley et al. 2013) as a control field. The IRAC fluxes in the UDS catalog were deblended using the same method described above, using the resolved $K_s$ images to deblend sources (see Hartley et al. 2013). The UDS has $5\sigma$ depths of $i' = 27.0$ mag, $J = 24.9$ mag, $[3.6] = 24.2$ mag and $[4.5] = 24.0$ mag (Furusawa et al. 2008; Hartley et al. 2013). We therefore use the same magnitude cuts for the UDS as for the 7C 1753+6311 field. We do not consider Eddington bias due to the greater depth of the UDS, however we do not expect it to significantly affect our results, particularly regarding the fraction of the most massive galaxies in the cluster that are quiescent.

The UDS is a $K_s$-selected survey, whereas we use an F140W selection for 7C 1753+6311. Both selections are done in the infrared, and both are much deeper than our $J \leqslant 23.6$ mag selection so these methods are unlikely to differ greatly. They would only differ for extremely red sources with very faint F140W magnitudes and bright $K_s$ magnitudes. We have checked that the different selection methods do not affect our use of the UDS as a control sample by comparing number counts in the two fields as a function of $i'$, $J$, [3.6] and [4.5] magnitudes and find that they match well within the color and magnitude cuts stated above.

Where we compare the properties of the cluster galaxies to the field, we use only those galaxies selected in the UDS which have photometric redshifts between $1.5 < z < 1.7$.[14] This ensures we are comparing the cluster properties to those of the field at approximately the same redshift. For statistical subtraction (see below), we use the full UDS with no photometric redshift constraints.

#### 2.3.2. Subtraction of Field Contaminants

Since we do not identify cluster members with spectra or photometric redshifts, we use statistical subtraction to derive the cluster galaxy properties. The fore- and background population is estimated from ~400 random 0.9 arcmin radius regions in the UDS, having applied the same color and magnitude cuts as above. The field contribution is estimated from the median of these 400 regions and then subtracted from the corresponding number of galaxies around 7C 1753+6311. The uncertainty is the $1\sigma$ standard deviation of the 400 field regions.

[14] Photometric redshifts determined from the full 11-band photometry of the UDS, see Hartley et al. (2013).

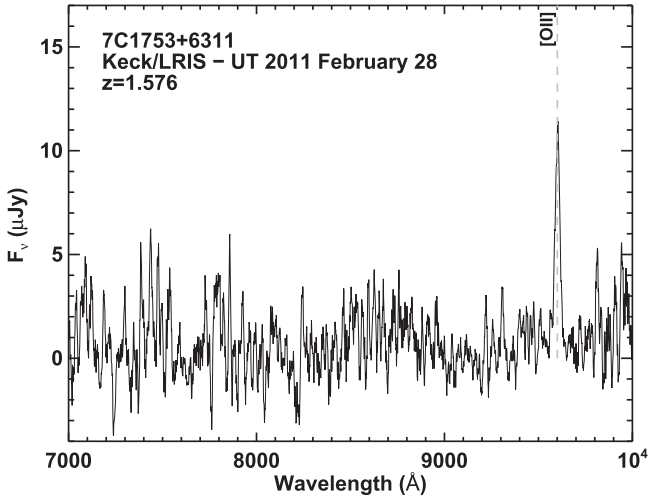


**Figure 2.** Keck/LRIS spectrum of 7C 1753+6311 obtained on UT 2011 February 28 (smoothed with a boxcar average of 10 Å for clarity). A single, high equivalent width emission line is detected at 9602 Å which we identify as the [O II] $\lambda$3727 doublet which places 7C 1753+6311 at $z = 1.576$. This redshift is confirmed with corresponding H$\alpha$ emission by A. E. Rettura et al. (2016, in preparation).

## 3. REDSHIFT OF 7C 1753+6311

We obtained a deep optical spectrum of 7C 1753+6311 using the Low Resolution Imaging Spectrometer (LRIS; Oke et al. 1995) at the Keck I telescope during twilight on UT 2011 February 28. LRIS is a double spectrograph, and we integrated for 1200 s on the blue arm and 1120 s on the red arm in order to match read-out times. The observations used the 1.″5 wide longslit and the data were processed using standard procedures and flux calibrated using an archival sensitivity function from 2011 April. Nothing is detected on the blue side, but a single, strong, high equivalent width emission line is detected at 9602 Å on the red side, which we identify with the [O II] $\lambda$ 3727 doublet at $z = 1.576$ (see Figure 2). For the instrument configuration we used, the spectral resolving power was $R \equiv \lambda/\Delta\lambda = 1600$ for objects filling the slit at ~9600 Å, which is insufficient to resolve the [O II] doublet. However, the redshift is confirmed by the detection of corresponding H$\alpha$ emission in a Keck near-infrared spectrum reported by A. E. Rettura et al. (2016, in preparation). In comparison to radio galaxies surrounded by protoclusters typically reported in the literature (e.g., Venemans et al. 2007; Galametz et al. 2010; Hatch et al. 2011), this is a relatively weak line emitter. We do not find any features at 4854 Å and this wavelength does not correspond to any strong spectral features for our measured redshift. The feature noted in Lacy et al. (1999) was therefore probably due to noise in their shallow data.

## 4. CLUSTER PROPERTIES

### 4.1. A Galaxy Cluster at $z = 1.58$

Figure 3 shows a density map of the field around 7C 1753 +6311 and ClG 0218.3−0510, a well-studied cluster at $z = 1.62$ (Papovich et al. 2010; Tanaka et al. 2010). These maps were produced by measuring the number density of sources (selected using the color and magnitude criteria described in Section 2) within 30 arcsec radius apertures around each 5 arcsec pixel. The UDS was mapped in the same way, and the mean and standard deviation of densities in the

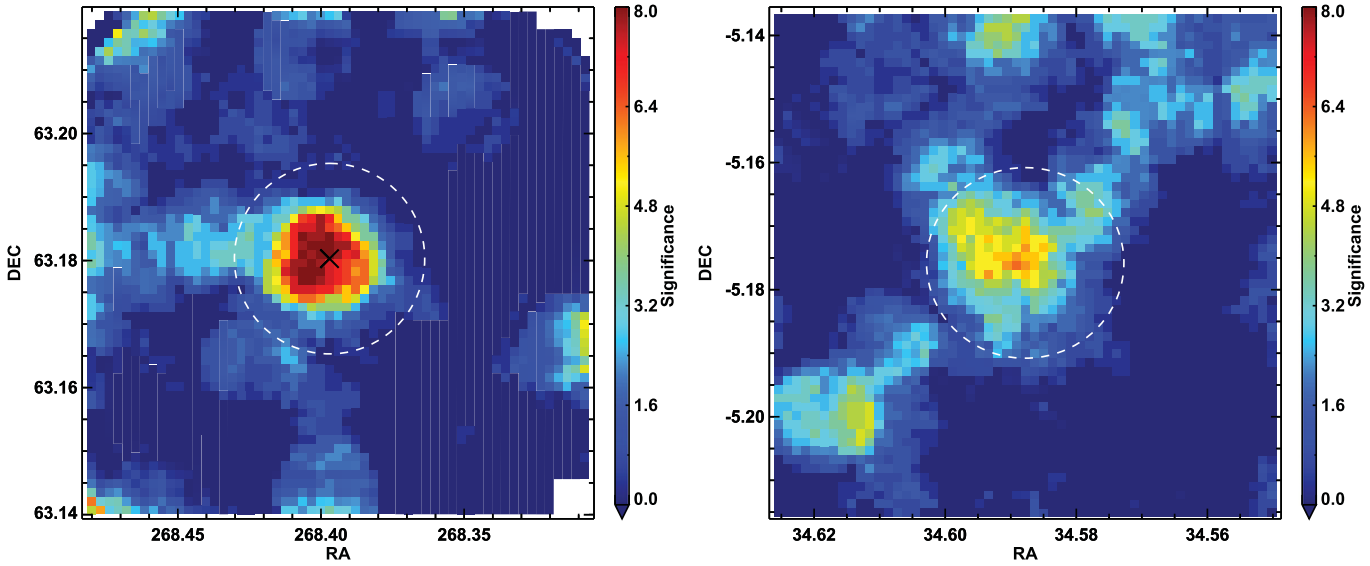


**Figure 3.** Left: density map of color-selected sources in CARLA J1753+6311. The *HST* image used to detect sources has been supplemented by the $i'$ and $J$ images in the outskirts to show the extended field around 7C 1753+6311. The RLAGN is shown by the black cross and the circle shows a 0.9 arcmin radius around the RLAGN. Only sources within this circle are considered in this paper. The colorbar shows the overdensity in sigma compared to the average field. Right: density map of color-selected sources in ClG 0218.3−0510. The white circle has a radius of 0.9 arcmin around the center of the cluster, as measured by Papovich et al. (2010).

UDS were used to convert each number density value to a significance above the expected field density. The pixels in Figure 3 are therefore correlated as each 5 arcsec pixel indicates the overdensity within a 30 arcsec radius aperture. Using the selection criteria defined in Section 2, the peak overdensity around 7C 1753+6311 is an $8.9\sigma$ significance of galaxies within a 30 arcsec aperture, centered 16 arcsec (136 kpc) from the radio galaxy. These galaxies appear to be highly clustered around the central RLAGN (Figure 1). The source density is so high in the central 0.9 arcmin region that five pairs of sources were blended in the 4.5 $\mu$m image, and their true nature was only discovered in the higher resolution ground-based data. It is possible that many of the other CARLA cluster candidates which have extremely high galaxy overdensities also suffer from blending.

Follow-up near-infrared Keck spectroscopy of 7C 1753 +6311 revealed five galaxies, including the RLAGN, with spectroscopic redshifts between $1.578 < z < 1.587$ within a projected diameter of 2 Mpc (A. E. Rettura et al. 2016, in preparation). This structure therefore satisfies the criteria set out by Eisenhardt et al. (2008) for a spectroscopically confirmed $z > 1$ (proto)cluster, and so we refer to the structure as CARLA J1753+6311 from now on.

Besides the RLAGN, there are $29 \pm 6$ excess galaxies within 0.9 arcmin of 7C 1753+6311 that are selected with the above color and magnitude criteria.[15] This level of clustering and overdensity is slightly greater than that of the ClG 0218.3 −0530 protocluster at $z = 1.62$, which has a galaxy excess of $22 \pm 6$ using the same criteria. The cluster ClG 0218.3−0530 is a well-studied structure with a tentative $4.5\sigma$ X-ray detection potentially indicating a collapsed core (Tanaka et al. 2010). The comparably high galaxy overdensity surrounding 7C 1753 +6311 (Figure 3) suggests that this RLAGN is surrounded by a protocluster consisting of a dominant main halo that is already a relatively high-mass group.

The approximate mass of CARLA J1753+6311 can be estimated from the galaxy richness. Andreon & Congdon (2014a) reported that galaxy richness was a good proxy for cluster mass, with little dependence on redshift. ClG 0218.3 −0530 has an X-ray determined mass of 4–8 $\times 10^{13} M_{\odot}$ (Tanaka et al. 2010; Pierre et al. 2012), which is consistent with the galaxy velocity dispersion (Tran et al. 2015). Since CARLA J1753+6311 is richer than ClG 0218.3−0530, its mass is likely to be slightly greater. Using Equation (3) from Andreon & Congdon (2014a), and the calculated value of $m^*_{4.5\,\mu\mathrm{m}} + 1 = 21.2$ from Wylezalek et al. (2014) we measure a cluster richness of $10 \pm 1$ galaxies[16] with $[4.5] \leqslant 21.2$, and estimate the mass within 500 kpc of 7C 1753+6311 to be $(9.2 \pm 4.5) \times 10^{13} M_{\odot}$, consistent with this structure being a slightly more massive group than ClG 0218.3−0530.

### 4.2. Red Sequence and Red Fraction

One of the signs of a mature cluster is the presence of a red sequence. Ubiquitous in clusters at $z < 1$, red sequences persist in galaxy clusters out to at least $z = 1.4$ (Stanford et al. 2005; Snyder et al. 2012), and have been found in some dense (proto) clusters at even higher redshifts (e.g., Kodama et al. 2007; Stanford et al. 2012; Newman et al. 2014).

In Figure 4 we show the $i' - J$ color–magnitude diagram of sources within 0.9 arcmin of the RLAGN (∼500 kpc at this redshift).[17] Larger squares indicate sources that are within 30 arcsec of the radio galaxy. The histogram in the top panel of Figure 4 shows the excess number of galaxies in CARLA J1753+6311, compared to the UDS control field. There is a significant overdensity in the field around 7C 1753 +6311 at all magnitudes, increasing at the faint end. Although

[15] The number of excess galaxies was calculated by taking the number of field galaxies selected in 400 random 0.9 arcmin fields in the UDS and subtracting this from the number of galaxies selected around 7C 1753+6311, then taking the mean and standard deviation of the resultant distribution.

[16] This is the number of background-subtracted galaxies in the 7C 1753 +6311 field.

[17] None of our results qualitatively change when we consider a smaller 30 arcsec radius field.

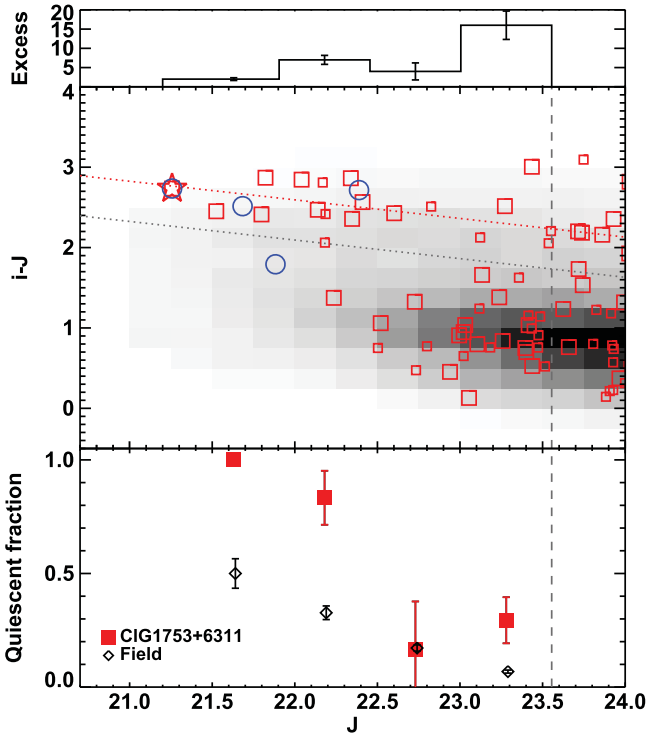


**Figure 4.** Top: histogram showing the number of excess sources within 0.9 arcmin of 7C 1753+6311 compared to the expected numbers in a random blank field, as a function of $J$ band magnitude. Middle: color–magnitude diagram showing a clear structure of red sources at $i' - J \sim 2.5$. The RLAGN is marked with a red star. All sources within 0.9 arcmin of the RLAGN are marked with red squares. Larger squares indicate those within 0.5 arcmin of the RLAGN. The gray dashed line indicates the $3\sigma$ depth of the $J$ band. The best fit to the red sequence is shown by the red dotted line. The gray dotted line indicates 0.5 mag below this line. The background grayscale shows the normalized distribution of the UDS for comparison. Spectroscopic members (A. E. Rettura et al. 2016, in preparation) are highlighted with large blue circles. Bottom: the quiescent fraction of galaxies in CARLA J1753+6311 as a function of $J$ band magnitude. Red squares show the cluster values, black diamonds indicate the quiescent fractions measured for field galaxies.

we expect contamination from fore- and background field sources in the color–magnitude diagram, the majority of the red data points are likely to be cluster members, and there is a clear, strong red sequence at $J < 23$ mag, with hints of the sequence continuing to fainter magnitudes.

The red sequence is fit by the line $i' - J = 7.688 - 0.232 \times J$, calculated by iteratively clipping sources more than $1.5\sigma$ from the best-fit line, allowing both the slope and normalization to freely vary, until convergence was reached. The fit is shown by the red dotted line in Figure 4. The colors of sources on this red sequence suggest they formed at redshifts of $2 < z_f < 3$, assuming the galaxies formed their stars in single bursts. A cluster formation model in which the member galaxies formed over the course of 2–3 Gyr, with galaxy formation peaking at $z = 3$ predicts an average red sequence color of $i' - J = 2.7$ mag, consistent with the data (Cooke et al. 2015).

We define "red" galaxies as those that lie within 0.5 mag of (or redder than) the red sequence (shown by the lower, gray, dotted line in Figure 4); this cleanly divides the red sequence from the blue cloud. We calculate the red fraction for CARLA J1753+6311, statistically removing the expected number of field contaminants as:

$$f_{\rm red} = \left\langle \frac{\left(N_{\rm red}^{\rm 7C1753} - N_{\rm red}^{\rm field}\right)}{\left(N_{\rm total}^{\rm 7C1753} - N_{\rm total}^{\rm field}\right)} \right\rangle_{\rm median} \quad (1)$$

where $N_{\rm red}^{\rm field}$ and $N_{\rm total}^{\rm field}$ are the measured number of "red" and total galaxies that satisfy our color criteria in ~400 random 0.9 arcmin field regions from the UDS. The uncertainty is the $1\sigma$ standard deviation in the calculated red fractions for CARLA J1753+6311.

The fraction of red galaxies in the protocluster is significantly larger than in the blank field. The red fraction of CARLA J1753+6311, after statistically removing field contaminants, is $f_{\rm red} = 0.66 \pm 0.13$, compared to the average fraction of $1.5 < z < 1.7$ galaxies in the UDS control field, which is $f_{\rm red} = 0.27 \pm 0.01$ (see Table 1). CARLA J1753+6311 has a similar red fraction to the $z = 1.62$ protocluster ClG 0218.3−0510, which has $f_{\rm red} = 0.48 \pm 0.15$. So the enhanced red fraction in CARLA J1753+6311 seems typical for mature protoclusters. The dense environment of the protoclusters appears to have a strong impact on the colors of their member galaxies.

**Table 1**
Fractions of Quiescent Galaxies in CARLA J1753+6311, ClG 0218.3−0510 and in the Control Field UDS at $1.5 < z < 1.7$

| | CARLA J1753 +6311 | ClG0218.3 −0510 | UDS |
|---|---|---|---|
| $f_{\rm red}$ | $0.66 \pm 0.13$ | $0.48 \pm 0.15$ | $0.27 \pm 0.01$ |
| $f_{\rm Q}$ ($J \leqslant 23.6$) | $0.50 \pm 0.09$ | $0.30 \pm 0.08$ | $0.16 \pm 0.01$ |
| $f_{\rm Q}$ (red galaxies) | $0.80 \pm 0.06$ | $0.67 \pm 0.11$ | $0.61 \pm 0.03$ |
| $f_{\rm Q}$ ($M_* \geqslant 10^{10} M_\odot$) | $0.76 \pm 0.13$ | $0.44 \pm 0.14$ | $0.28 \pm 0.01$ |
| $f_{\rm Q}$ ($M_* \geqslant 10^{10.5} M_\odot$) | $0.91 \pm 0.09$ | $0.38 \pm 0.16$ | $0.36 \pm 0.02$ |

**Note.** $f_{\rm Q}$ gives the quiescent galaxy fraction and $f_{\rm red}$ gives the fraction of galaxies with red colors in each sample.

### 4.3. Quiescent Galaxy Fraction

In low-redshift clusters the galaxies that lie on the red sequence are predominantly passively evolving, old galaxies. However, dusty star-forming galaxies (with $A_V \sim 1$–3) exhibit colors similar to those expected from quenched, passively evolving (i.e., quiescent) galaxies, and these galaxies make up approximately half of the red infrared-selected galaxy population at higher redshifts (Kriek et al. 2008). Furthermore, recent literature has also shown that high-redshift clusters and protoclusters do contain dusty star-forming galaxies (e.g., Brodwin et al. 2013; Dannerbauer et al. 2014; Smail et al. 2014; Santos et al. 2015). The enhanced red fraction of sources in CARLA J1753+6311 could therefore be ascribed to an excess of dusty star-forming galaxies and/or quenched, passively evolving galaxies. Here we use the rest-frame $U$, $B$, $J$ colors (observed $i'$, $J$, [3.6]) to separate these two populations.

Using the method outlined in Williams et al. (2009), Papovich et al. (2012) used the observed-frame $z'$, $J$ and 3.6 $\mu$m bands (rest-frame $U$, $B$, $J$) to separate galaxies in the $z = 1.62$ cluster ClG 0218.3−0510 into quiescent and star-forming populations. Using the full SED fits to the ClG 0218.3−0510 cluster members, we have converted the

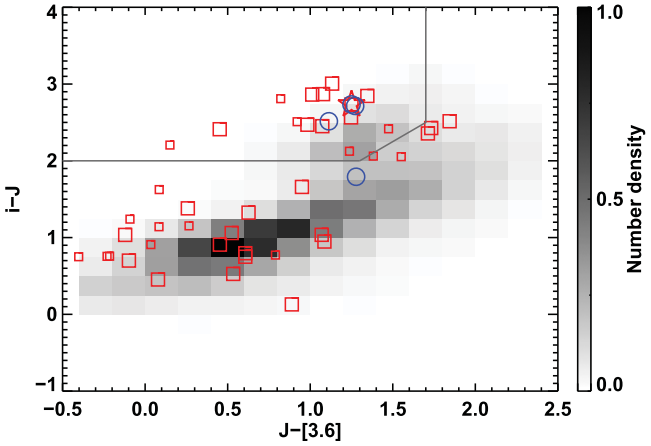


**Figure 5.** Observed $i' - J$ vs. $J - [3.6]$ (rest-frame $U - B$ vs. $B - J$) color–color diagram. The upper left quadrant selects quiescent galaxies at $z \sim 1.6$. Sources further toward the upper-right are dusty star-forming objects and those at bluer $i' - J$ colors are star-forming galaxies. The background density map shows the expected normalized distribution of field sources from the UDS. The symbols are the same as in Figure 4.

Papovich et al. (2012) selection criteria to use our $i'$, $J$, and 3.6 $\mu$m bands. Quiescent galaxies are those which satisfy the following (slightly stricter) criteria:

$$i' - J \geqslant 2.0 \quad (2)$$

$$J - [3.6] \leqslant 1.7 \quad (3)$$

$$i' - J \geqslant 0.375 + 1.25 \times (J - [3.6]). \quad (4)$$

We caution the reader that these equations were derived specifically for the eighth data release of the UDS and our data. The 3.6 $\mu$m magnitudes may be systematically offset by up to 0.5 mag due to the method by which they were determined and so these criteria may change for different datasets.

Figure 5 shows the distribution of all sources selected in CARLA J1753+6311 in $i' - J$ versus $J - [3.6]$ (rest-frame $U - B$ versus $B - J$) color–color space. The grayscale shows the expected distribution of the control field. The lines show the $i'$, $J$, [3.6] criteria used to select quiescent galaxies, which lie in the upper-left quadrant. The full cluster membership of CARLA J1753+6311 is not known, so interlopers were statistically removed in $i'J[3.6]$ color–color space using the UDS as the control field. To do this we use ~400 random 0.9 arcmin radius regions in the UDS, classifying sources as "quiescent" or "star-forming" using the above criteria. Sources in the 7C 1753+6311 field are then classified as "quiescent" or "star-forming," and the quiescent fraction calculated as:

$$f_{\rm Q} = \left\langle \frac{\left(N_{\rm Q}^{\rm 7C1753} - N_{\rm Q}^{\rm field}\right)}{\left(N_{\rm total}^{\rm 7C1753} - N_{\rm total}^{\rm field}\right)} \right\rangle_{\rm median} \quad (5)$$

where $N_{\rm Q}^{\rm field}$ is the measured number of rest-frame *UBJ*-selected quiescent galaxies in ~400 random 0.9 arcmin field regions. The uncertainty is the $1\sigma$ standard deviation in the calculated quiescent fractions for CARLA J1753+6311.

Without far-IR data, we are unable to locate extremely dust-obscured systems, so these will not be found in either the 7C 1753+6311 field or UDS and would be missing from Figure 5. These extremely dusty galaxies are rare, but could be an important population in protoclusters (e.g., Brodwin et al. 2013). In addition, some galaxies (of order ~10%) may be misclassified due to very dusty regions within them. Further analysis with submillimeter data would be required to examine the extremely dusty populations in these fields. This means that we cannot analyze the extremely dust-obscured populations in any of the fields considered here, but we are able to do a robust comparison between them as the dusty populations are undetected in all of these fields: CARLA J1753+6311, ClG 0218.3−0510 and the UDS control field.

Half of the detected galaxies in CARLA J1753+6311 are quiescent, with a quiescent fraction ($f_{\rm Q}$) for sources with $J \leqslant 23.6$ of $f_{\rm Q} = 0.50 \pm 0.09$ (see Table 1). Of the "red" galaxies, $80 \pm 6\%$ are quiescent, so the vast majority of these objects are not dust-obscured star-forming galaxies, but are already quenched and evolving passively.

ClG 0218.3−0510 contains fewer passively evolving galaxies ($f_{\rm Q} = 0.30 \pm 0.08$), with $67 \pm 11\%$ of the red galaxies classified as quiescent. These fractions were calculated using the same criteria as in Section 2 and within a 0.9 arcmin aperture of the cluster core. CARLA J1753+6311 has a similar fraction of red, quiescent galaxies at a $1\sigma$ level.

Both of these protoclusters contain a significantly higher quiescent fraction than the average field, which is $f_{\rm Q} = 0.16 \pm 0.01$. This means that the star formation rates of many cluster members are greatly suppressed relative to the field.

### 4.4. Passive Fraction as a Function of Mass

The quiescent fraction is a strong function of $J$ band magnitude. As shown in the bottom panel of Figure 4, the quiescent fraction gradually rises with decreasing magnitude. At $J < 22.5$ mag the fraction of quiescent galaxies in the protocluster rises to >80%, double the field fraction.

The [4.5] flux provides a better correlation with stellar mass than the $J$ flux, and is nearly independent of galaxy type. Using galaxies with known stellar masses (from full SED-fitting) in the UDS (Mortlock et al. 2013), we convert the [4.5] magnitudes to stellar mass using $\log(M_*/M_\odot) = 22.53 - 0.57 \times [4.5]$. This equation was derived empirically by fitting a line to the stellar masses and [4.5] magnitudes from the UDS, which was resampled to have the same $J \leqslant 23.6$ quiescent fraction as CARLA J1753+6311, i.e., 50%, to remove the slight dependence of this relation on galaxy type. This line has an intrinsic scatter of 0.2 dex. We use this equation to calculate the masses for CARLA J1753+6311. We use a similar equation but for the full UDS with no resampling, to calculate the masses for the field. This simply corresponds to a slight shift in the bin center in Figure 6. Using these equations, we recalculate the quiescent fractions as a function of stellar mass (Figure 6). These fractions were calculated as in Section 4.3 for sources in [4.5] magnitude bins (corresponding to stellar mass).

There is also a strong correlation between galaxy mass and passivity, with a higher fraction of the massive sources being quiescent. Figure 6 shows that this trend is steeper for the protocluster galaxies than for the field galaxies, and there is a divide at $M_* \sim 10^{10.5} M_\odot$. Only 20%–30% of galaxies with stellar masses $M_* < 10^{10.5} M_\odot$ are quiescent in both environments, whereas 80%–100% of $M_* > 10^{10.5} M_\odot$ galaxies are quiescent in the protocluster, compared to only ~40% in the field (Table 1).

We find that the fraction of quiescent galaxies is dependent on environment: CARLA J1753+6311 contains double the quiescent fraction of the control field at $z \sim 1.6$. However, this

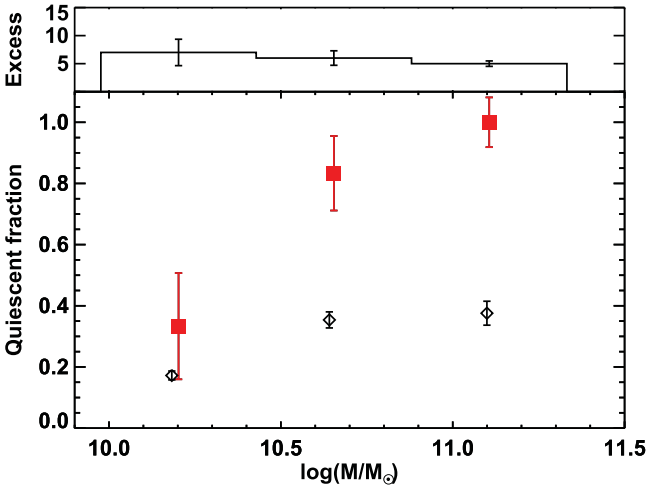


**Figure 6.** Quiescent fraction measured in 4.5 $\mu$m magnitude bins, which correspond to stellar mass bins. Red squares show the cluster values, black diamonds indicate the quiescent fractions measured for field galaxies. The top histogram shows the excess number of sources in CARLA J1753+6311, compared to a random blank field, per mass bin.

environmental effect is also mass dependent: only the population of high-mass galaxies has an enhanced quenched fraction relative to the control field. These results are consistent with recent literature on red galaxies in clusters at $z > 1.5$. Rudnick et al. (2012) and Fassbender et al. (2014) found a strong excess of bright, red galaxies in two $z \sim 1.6$ clusters, but a corresponding lack of faint, red galaxies. However, in contrast to these results, Andreon et al. (2014b) found a well-populated red sequence down to $\sim 10^{10} M_\odot$ in a $z \sim 1.8$ cluster and Lee et al. (2015) find that there is no difference in the quiescent fraction between cluster and field environments at $z > 1$, with a large variation between individual clusters. Therefore the mass dependence of quiescent galaxies needs to be analyzed in a larger sample of protoclusters to draw firm conclusions.

In van der Burg et al. (2013) clusters at $z \sim 1$ were also shown to have an increased quiescent fraction compared to the field. The quiescent fractions in CARLA J1753+6311 are similar to the $z \sim 1$ fractions at high masses ($M > 10^{10.5}\ M_\odot$), which is further evidence that CARLA J1753+6311 is already a very mature structure, more similar to $z = 1$ clusters than higher redshift protoclusters. The quiescent fraction at lower masses is much higher at $z \sim 1$ than in CARLA J1753+6311. This may suggest a build up of the low mass end of the red sequence in clusters from $z = 1.6$ to $z = 1$.

## 5. CONCLUSIONS

We present the first robust spectroscopic redshift of the high redshift RLAGN 7C 1753+6311, placing it at $z = 1.58$. We show this radio galaxy is located in an $8.9\sigma$ galaxy overdensity, implying that it is embedded in a high redshift galaxy cluster. The cluster core contains $28 \pm 6$ excess galaxies brighter than $J = 23.6$ mag. This galaxy richness implies a cluster mass of at least several $\times 10^{13} M_\odot$. Of these excess galaxies, $66 \pm 13\%$ have red colors and lie on a sequence in color–magnitude space. The rest-frame *UBJ* colors of these galaxies show that 80% of the red galaxies are quiescent, therefore this is a mature cluster with a predominantly old stellar population. More than 80% of the galaxies with masses $M_* > 10^{10.5} M_\odot$ are quiescent in this cluster, compared to only ~40% of field galaxies of this high mass. At lower masses we find no difference between the quiescent fractions of the field and cluster galaxies. This mature structure is similar in the level of clustering, overdensity and red fraction to other clusters at a similar redshift. The presence of a dense core and a well-formed, passively evolving red sequence suggest that RLAGN do not solely reside in young, uncollapsed protoclusters, rather they can be used as beacons for clusters in a wide range of evolutionary states.

The authors would like to thank Omar Almaini for making the UDS catalogs and images available and the staff at the WHT for taking the service mode observations. We thank the anonymous referee for their careful review of the manuscript and their helpful comments which improved the content of the paper.

E.A.C. acknowledges the support of the STFC. N.A.H. is supported by an STFC Rutherford Fellowship. The work of D.S. was carried out at the Jet Propulsion Laboratory, California Institute of Technology, under a contract with NASA.

This work was based on observations made with the William Herschel Telescope under programme IDs W/2013b/10 and SW2015a07 and with the *Spitzer Space Telescope*. The William Herschel Telescope and its service programme are operated on the island of La Palma by the Isaac Newton Group in the Spanish Observatorio del Roque de los Muchachos of the Instituto de Astrofísica de Canarias. *Spitzer* is operated by the Jet Propulsion Laboratory, California Institute of Technology under a contract with NASA. Support for this work was provided by NASA through an award issued by JPL/Caltech.

Some of the data presented herein were obtained at the W.M. Keck Observatory, which is operated as a scientific partnership among the California Institute of Technology, the University of California and the National Aeronautics and Space Administration. The Observatory was made possible by the generous financial support of the W.M. Keck Foundation. The authors wish to recognize and acknowledge the very significant cultural role and reverence that the summit of Mauna Kea has always had within the indigenous Hawaiian community. We are very grateful to have the opportunity to conduct observations from this mountain.

## REFERENCES

Andreon, S., & Congdon, P. 2014a, A&A, 568, A23
Andreon, S., Newman, A. B., Trinchieri, G., et al. 2014b, A&A, 565, A120
Bertin, E., & Arnouts, S. 1996, A&AS, 117, 393
Bleem, L. E., Stalder, B., de Haan, T., et al. 2015, ApJS, 216, 27
Brodwin, M., Gonzalez, A. H., Stanford, S. A., et al. 2012, ApJ, 753, 162
Brodwin, M., Stanford, S. A., Gonzalez, A. H., et al. 2013, ApJ, 779, 138
Chiang, Y.-K., Overzier, R., & Gebhardt, K. 2013, ApJ, 779, 127
Chiang, Y.-K., Overzier, R., & Gebhardt, K. 2014, ApJL, 782, L3
Cooke, E. A., Hatch, N. A., Muldrew, S. I., Rigby, E. E., & Kurk, J. D. 2014, MNRAS, 440, 3262
Cooke, E. A., Hatch, N. A., Rettura, A., et al. 2015, MNRAS, 452, 2318
Dannerbauer, H., Kurk, J. D., De Breuck, C., et al. 2014, A&A, 570, A55
Eisenhardt, P. R. M., Brodwin, M., Gonzalez, A. H., et al. 2008, ApJ, 684, 905
Erben, T., Schirmer, M., Dietrich, J. P., et al. 2005, AN, 326, 432
Fassbender, R., Nastasi, A., Santos, J. S., et al. 2014, A&A, 568, A5
Fazio, G. G., Hora, J. L., Allen, L. E., et al. 2004, ApJS, 154, 10
Furusawa, H., Kosugi, G., Akiyama, M., et al. 2008, ApJS, 176, 1
Galametz, A., Stern, D., De Breuck, C., et al. 2012, ApJ, 749, 169
Galametz, A., Stern, D., Stanford, S. A., et al. 2010, A&A, 516, A101
Hartley, W. G., Almaini, O., Mortlock, A., et al. 2013, MNRAS, 431, 3045
Hasseleld, M., Hilton, M., Marriage, T. A., et al. 2013, JCAP, 7, 8
Hatch, N. A., De Breuck, C., Galametz, A., et al. 2011, MNRAS, 410, 1537

Hatch, N. A., Wylezalek, D., Kurk, J. D., et al. 2014, MNRAS, 445, 280
Kodama, T., Tanaka, I., Kajisawa, M., et al. 2007, MNRAS, 377, 1717
Kriek, M., van Dokkum, P. G., Franx, M., et al. 2008, ApJ, 677, 219
Lacy, M., Rawlings, S., Hill, G. J., et al. 1999, MNRAS, 308, 1096
Lee, S.-K., Im, M., Kim, J.-W., et al. 2015, ApJ, 810, 90
Mortlock, A., Conselice, C. J., Hartley, W. G., et al. 2013, MNRAS, 433, 1185
Muldrew, S. I., Hatch, N. A., & Cooke, E. A. 2015, MNRAS, 452, 2528
Muzzin, A., Wilson, G., Yee, H. K. C., et al. 2009, ApJ, 698, 1934
Newman, A. B., Ellis, R. S., Andreon, S., et al. 2014, ApJ, 788, 51
Oke, J. B., Cohen, J. G., Car, M., et al. 1995, PASP, 107, 375
Orsi, A. A., Fanidakis, N., Lacey, C. G., & Baugh, C. M. 2015, arXiv:1509.01254
Overzier, R. A., Harris, D. E., Carilli, C. L., et al. 2005, A&A, 433, 87
Papovich, C. 2008, ApJ, 676, 206
Papovich, C., Momcheva, I., Willmer, C. N. A., et al. 2010, ApJ, 716, 1503
Papovich, C., Bassett, R., Lotz, J. M., et al. 2012, ApJ, 750, 93
Pierre, M., Clerc, N., Maughan, B., et al. 2012, A&A, 540, A4
Planck Collaboration et al. 2015, arXiv:1502.01598
Rettura, A., Martinez-Manso, J., Stern, D., et al. 2014, ApJ, 797, 109
Rudnick, G. H., Tran, K.-V., Papovich, C., Momcheva, I., & Willmer, C. 2012, ApJ, 755, 14
Santos, J. S., Altieri, B., Valtchanov, I., et al. 2015, MNRAS, 447, L65
Schirmer, M. 2013, ApJS, 209, 21
Simpson, C., & Eisenhardt, P. 1999, PASP, 111, 691
Simpson, C., & Rawlings, S. 2002, MNRAS, 334, 511
Smail, I., Geach, J. E., Swinbank, A. M., et al. 2014, ApJ, 782, 19
Snyder, G. F., Brodwin, M., Mancone, C. M., et al. 2012, ApJ, 756, 114
Stanford, S. A., Eisenhardt, P. R., Brodwin, M., et al. 2005, ApJL, 634, L129
Stanford, S. A., Brodwin, M., Gonzalez, A. H., et al. 2012, ApJ, 753, 164
Stanford, S. A., Gonzalez, A. H., Brodwin, M., et al. 2014, ApJS, 213, 25
Tanaka, M., Finoguenov, A., & Ueda, Y. 2010, ApJL, 716, L152
Tozzi, P., Santos, J. S., Jee, M. J., et al. 2015, ApJ, 799, 93
Tran, K.-V. H., Nanayakkara, T., Yuan, T., et al. 2015, ApJ, 811, 28
Van Breukelen, C., Simpson, C., Rawlings, S., et al. 2009, MNRAS, 395, 11
van der Burg, R. F. J., Muzzin, A., Hoekstra, H., et al. 2013, A&A, 557, A15
Venemans, B. P., Rottgering, H. J. A., Miley, G. K., et al. 2007, A&A, 461, 823
Williams, R. J., Quadri, R. F., Franx, M., van Dokkum, P., & Labbé, I. 2009, ApJ, 691, 1879
Willis, J. P., Clerc, N., Bremer, M. N., et al. 2013, MNRAS, 430, 134
Wylezalek, D., Galametz, A., Stern, D., et al. 2013, ApJ, 769, 79
Wylezalek, D., Vernet, J., De Breuck, C., et al. 2014, ApJ, 786, 17